Structural Transitions in Amorphous Water Ice and Astrophysical Implications

Peter Jenniskens and David F. Blake

Selected area electron diffraction is used to monitor structural changes of vapor-deposited water ice in vacuum during warm-up from 15 to 188 K. A progression of three amorphous forms of water ice is found with well-defined transitions. The formation of a high-density amorphous form (I_ah) at 15 K is confirmed, and the transition to the more familiar low-density form (I_al) occurs gradually over the range 38 to 68 K. At 131 K, the ice transforms into a third amorphous form (I_ar), which precedes the crystallization of cubic ice (I_c) and coexists metastably with I_c from 148 K until at least 188 K. These structural transformations of amorphous water ice can be used to explain hitherto anomalous properties of astrophysical ices. The structural transition from I_ah to I_al is responsible for the diffusion and recombination of radicals in ultraviolet-photolyzed interstellar ices at low temperatures. The occurrence and persistence of I_ar explains anomalous gas retention and gas release from water-rich ices at temperatures above 150 K.

Amorphous water ice, vapor-deposited and with trapped impurities, plays an important role in astrophysics (1, 2). Such ice is observed spectroscopically as a frost on interstellar dust in dense molecular clouds and constitutes the bulk of matter in comets (1, 2). Amorphous water ice has relevance, too, in biological electron microscopy and cryobiology, where it is used as an embedding material replacing liquid water (3), and in the study of the structure and physical properties of liquid water itself (4–6). The experiments described here, although relevant to all of these areas, were designed to help interpret the complex outgassing phenomena observed in laboratory studies of cometary ice analogs and the diffusion of radicals found in experiments that simulate interstellar ices. These studies usually monitor gas release (7) or infrared absorption bands (8, 9) during a gradual warming of ice layers. Such phenomena are most likely related to changes in the structure of the water matrix, but structural changes are not directly observed.

We have recently combined selected area electron diffraction (SAED) and cryogenic techniques in an instrumental configuration that allows direct observation of the water ice structure as it evolves during warm-up under experimental conditions similar to those described above. Water vapor is deposited onto a 15 K amorphous carbon film inside a Hitachi H-500 H transmission electron microscope at a base pressure of 2×10^{-7} torr (10). The resulting ice film (~0.05 μm thick) (11) is warmed at the rate of 1 to 2 K per minute, and diffraction patterns are collected at 1-min intervals and stored digitally during warm-up. These diffraction patterns are then converted into radial intensity distributions

National Aeronautics and Space Administration Ames Research Center, Space Science Microscopy Laboratory, Mail Stop 239-4, Moffett Field, CA 94035, USA.

(Fig. 1). The momentum transfer coordinate ($k = 2\pi/d$, where d is the lattice spacing) is calibrated with patterns of crystalline gold deposited on a small part of the substrate. The relatively small intensity contributed by the amorphous carbon substrate is removed by a background subtraction algorithm.

Water ice that is formed by vapor deposition at low pressure has three established forms: two crystalline forms, the hexagonal (I_h) and cubic (I_c) polymorphs and a low-density amorphous form—I_al (our notation)—with a local density of 0.94 g/cm³ (4). In addition, Narten et al. (12) described a high-density (1.07 g/cm³) amorphous form of water ice (I_ah) made by vapor deposition at 10 K. The oxygen-oxygen radial distribution functions derived from x-ray diffraction patterns were found consistent with a structure similar to low-density amorphous ice but with additional interstitial water molecules.

We confirm the formation of a high-density amorphous form when water vapor is deposited on an amorphous carbon film at 15 K. Our diffraction patterns are identical to those reported by Heide (3). Fourier transformation of the I_ah pattern confirms the presence of a peak between 3 and 4 Å in the oxygen-oxygen radial distribution function, indicative of interstitial water (12). Thus, the high-density amorphous form is not an artifact of epitaxial growth on an oriented single crystal surface as was later suggested (4, 13). We have followed the transformation of high- to low-density amorphous ice by monitoring the position of the first and second diffraction maxima. The high-density form I_ah persists until about 38 K and then undergoes a well-defined, albeit sluggish, transition to the low-density amorphous form I_al in the temperature regime of 38 to 68 K (Fig. 2).

When the temperature T is increased

further, an irreversible change in structure of the low-density amorphous form occurs, marked by an increase in intensity and a slight sharpening of the first diffraction maximum. The structure starts to change before any sign of crystallinity in either the diffraction pattern or the bright-field images and has a well-defined onset at 131 ± 2 K for given experimental conditions (Fig. 3). In other experiments with heating rates of 1 to 2 K per minute but different annealing times, the onset of this transformation occurs between 122 and 136 K. The onset of crystallization occurs at 148 K (142 to 160 K in other experiments), during which the cubic 220 and 311 peaks appear (Fig. 1), the pattern becomes spotty, and crystallites emerge in the bright-field images. But most remarkably, within the time and temperature constraints of our experiments, the ice does not fully crystallize, a phenomenon first observed by Dowell and Rinfret (14). The magnitudes of the cubic diffraction maxima become, at best, similar to those of the amorphous component.
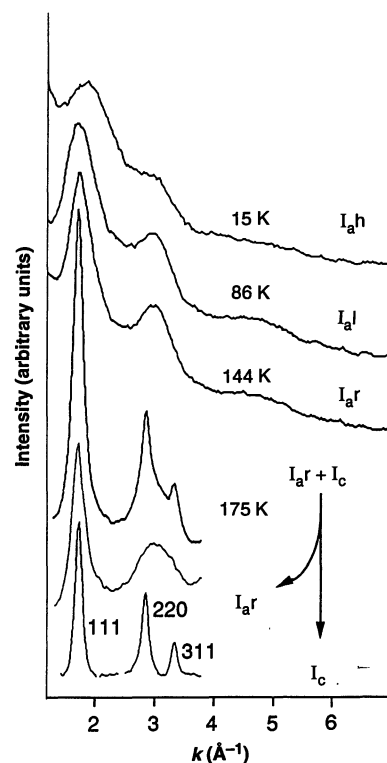
Fig. 1. Electron diffraction patterns of the different forms of vapor-deposited water ice from a region about 10 μm in diameter. The forms encountered are high-density amorphous ice (I_ah), low-density amorphous ice (I_al), restrained amorphous ice (I_ar) (while transforming from I_al), and a composite of restrained amorphous I_ar and cubic crystalline ice (I_c). The latter can be separated into two components by subtraction of a standard cubic pattern as indicated, which allows one to follow changes in the amorphous component after the onset of cubic crystallization.

The amorphous component of the pattern cannot be attributed to small crystallite size. The crystallites have sizes normally distributed about 0.05 to 0.15 μm. As the cubic diffraction pattern becomes more intense, the crystallites do not vary much in size and the half widths of the cubic diffraction maxima remain unaltered. These features are indicative of a structure transition rather than crystal growth (14). This constancy of crystal size allows us to separate the observed patterns into two components by subtracting an intensity-scaled pure cubic pattern. From this, we find that the amorphous component continues its gradual change as before the onset of crystallization until the rate of change of both cubic and amorphous components slows at 167 K (158 to 170 K in other experiments). Similar but smaller changes are observed in the width and position of both diffraction peaks. This behavior is consistent with a transition from the low-density amorphous form to another amorphous form, which we call $I_a r$. This form coexists with cubic crystals for at least 16 hours at 178 K. There is probably not a clear phase separation. Instead, we expect the amorphous component to be intimately mixed with cubic ice in the crystallites.

The ice layer becomes noticeably thinner as a result of sublimation at about 180 K and is lost at 188 K (188 to 212 K in other experiments). At higher confinement pressure, the recrystallization of cubic to hexagonal ice has been reported to start at 213 K (14). In the process, the amorphous component is converted to hexagonal ice (14), as can be deduced from published x-ray patterns (15).

The specific temperatures at which the transitions occur depend on the style of deposition, the deposition rate, and the presence of impurities (8). In our experiments, we found that the critical factors are the heating rate and the "annealing time," the time between deposition and the onset of the cubic transition. The values quoted here are for heating rates of 1 to 3 K per minute and annealing times of 1 to 2 hours.

An important question is whether the observed amorphous forms persist over extended periods of time. In time-dependency studies, the onset of crystallization occurs at exponentially increasing times for higher $1/T$. We derive an activation enthalpy of $\Delta H = 44 \pm 2$ kJ/mol, which is in agreement with previous studies (16, 17) and is about equal to the energy of two I_h hydrogen bonds per molecule (18). We find similar exponential behavior for the onset of amorphous form $I_a r$, with $\Delta H = 25 \pm 5$ kJ/mol. This creates a large region in the time-temperature diagram in which this amorphous form can persist. Preliminary results for the cubic to hexagonal recrystal-

lization indicate an activation enthalpy of $\Delta H \geq 50$ kJ/mol.

This brings us to the structure of amorphous form $I_a r$ of water. We propose the name "restrained" amorphous form ($I_a r$) because the structure of this form prevents large-scale reordering into the cubic polymorph (19). What type of short-range order would prevent restructuring into the cubic crystalline polymorph (before transformation into the hexagonal form at higher temperature or longer time)? A clue is provided from experiments in which amorphous ice is rapidly heated to 145 K and held at that temperature for several hours. Under these conditions, the diffraction patterns after the onset of cubic crystallization contain weak diffraction peaks characteristic of hexagonal ice I_h. Bright-field images of the 0.1-μm crystallites show numerous planar defects, occasionally with spacings <0.005 μm. We attribute these defects to local stacking disorder in which the normal ABCABC . . . stacking sequence of the cubic polymorph is interrupted by ABAB . . . domains typical of the hexagonal polymorph. These domains may have had their origin in the precursor amorphous ice $I_a r$.

We propose a model in which the $I_a l \rightarrow I_a r$ transition causes the water ice to relax into local domains of both hexagonal ABAB and cubic ABCABC closest packing. The ordering within these domains cannot extend beyond a few unit cells lest they would cause crystalline diffraction peaks (20). The activation enthalpy for the transition $I_a l \rightarrow I_a r$ suggests that this relaxation involves the breaking of one hydrogen bond per water molecule. The transition $I_a l \rightarrow I_c$ involves an activation enthalpy equivalent to the breaking of two hydrogen bonds per molecule. However, by

the formation of small hexagonally ordered domains during the relaxation, an even larger energy barrier is created that prevents crystallization $I_a r \nrightarrow I_c$ until all the ice rystallizes into the hexagonal polymorph I_h.

We have no time-dependency data on the high- to low-density amorphous ice transition that can be used to determine the activation enthalpy. The low temperature of the transition (starting at 38 K) suggests that ΔH is less than 10 kJ/mol. One possible reason for the existence of the transition $I_a h \rightarrow I_a l$ at such low temperature is that interstitial water allows five-coordination, which is thought to lower the activation enthalpy for restructuring (5).

Previous studies have suggested a third amorphous form, or even a phase, of amorphous water with an onset just before crystallization. In outgassing experiments, Kouchi observed an increase of vapor pressure at 133 K, which he interpreted as the result of a third amorphous phase called "I_{as}," also called "α-H_2O(III)" and "H_2O_{as}(III)" (7, 21). This interpretation was questioned by Sack and Baragiola (17), who argued that the observed pressure increase was caused by a combination of a high vapor pressure of the amorphous phase and disequilibrium temperatures from rapid heating. However, it is likely that $I_a r$ does have a higher vapor pressure than $I_a l$. It is not clear how $I_a r$ relates to Speedy's (22) hypothetical "water II," a phase that was proposed to link the quite different heat capacities of $I_a l$ and liquid water. It is also not clear how $I_a r$ relates to the glass transition that has been reported just before the onset of crystallization at 136 to 138 K (23). The cycling between 127 and 148 K needed to show the
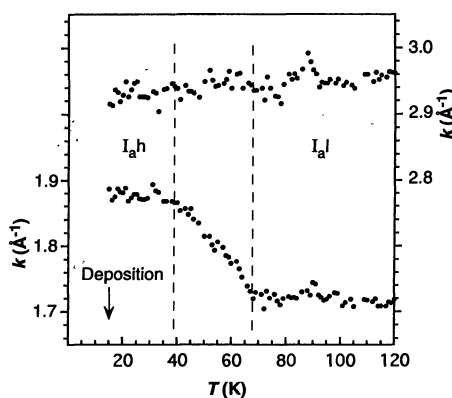
Fig. 2. Temperature dependence of the position of the first and second diffraction maxima in the temperature range in which amorphous water ice transforms from the high-density form to the low-density form. The transition is well defined, albeit sluggish. The ice was deposited at 15 K and held there for 37 min before warm-up at a rate of 2 K per minute.
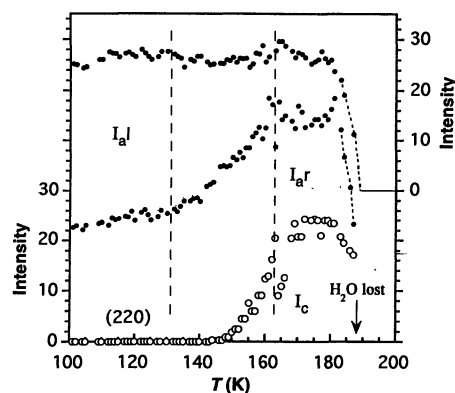
Fig. 3. Temperature dependence during warm-up of the intensity (in arbitrary units) of, from top to bottom, the second and first diffraction peaks of the amorphous component and the cubic 220 peak, which marks the onset of crystallization into I_c. The onset of the transition $I_a l \rightarrow I_a r$ is well defined by an increase in intensity of the first diffraction peak. The heating rate was 1 to 2 K per minute, and the onset of the cubic crystallization occurred 182 min after deposition at 15 K.

glass transition in differential scanning calorimetry suggests that the ice is in the $I_a r$ form when measured.

The existence of different, naturally occurring amorphous forms of water ice, each with a specific range of metastability, has important consequences in astrophysics. Observations of outgassing and diffusion of radicals in astrophysical ice analogs can be attributed to changes in the structure of the water ice matrix, which encloses the observed impurities. Indeed, for water-dominated ices we can make several observations.

Interstellar ice in cold ($T < 20$ K) dense molecular clouds is frozen on dust grains in an amorphous form. A good agreement of the position and width of the 3.07-μm infrared ice band with that of low-T deposits (8, 24) suggests that the ice is at least partially in the form $I_a h$. The $I_a h \rightarrow I_a l$ transition can play a role in the formation of solid reduced carbon. This proceeds through ultraviolet (UV) photolysis of H_2O, which creates mobile hydrogen atoms that are scavenged by carbon-containing impurities (for example, CO and CO_2). The resulting radicals recombine into more complex organic molecules called "organic residue" (25). This residue is subsequently processed into refractory material by additional UV photons (26). Figure 4 shows a laboratory simulation of this process in an experiment by Schutte (27), who traced the trapped impurities and radicals (HCO) by monitoring the strength of their infrared absorption bands during warm-up. Indeed,

the transition from high- to low-density amorphous ice is easily recognized in the diagram and coincides with a loss of HCO, ^{13}CO, and $^{13}CO_2$ infrared band strength (because of incorporation into larger organic species or outgassing). Therefore, small "organic residue" molecules may already be formed in the $I_a h \rightarrow I_a l$ transition, before the evaporation of the water matrix. This probably accounts for the relatively high efficiency of residue formation in laboratory studies (26, 27) and suggests an even greater efficiency of organic residue formation under astrophysical conditions. This is so because transient heating events could warm interstellar ice grains from the $I_a h$ regime into the $I_a l$ regime, causing radical recombination and residue formation. After cooling to the $I_a h$ regime, UV photons can transform the ice from the $I_a l$ form to the $I_a h$ form (3, 28) and create new radicals in the ice. Subsequent transient heating events could repeat the cycle many times over as long as traces of CO and CO_2 remain in the ice. Temperature fluctuations of low magnitude are much more abundant than those high enough to evaporate the water ice.

Comets are composed of primitive solar system ices. Two families of comets are known: Kuiper Belt objects, which remain during their lifetime at temperatures below 30 to 50 K, and Oort cloud objects, which were expelled from their formation zones in the Uranus-Neptune region where the ice was heated to some 60 to 100 K (2, 29). After being-expelled, the Oort cloud com-

ets cool down to temperatures $T < 20$ K but retain the structural signature of their higher temperature origin. Given this temperature history, we infer that the two classes of objects should have amorphous ice in two different forms: Kuiper Belt objects are made of high-density ice, whereas Oort cloud comets are made of low-density ice (but probably have a crust of high-density ice induced by cosmic-ray ion bombardment). "Density" in this context refers to the local ice structure and not to the mean volume density of the comet. The difference in ice structure may manifest itself in the outgassing characteristics of new comets. A small amount of outgassing associated with the amorphous to amorphous transitions is apparent in many lab experiments (7, 28). Finally, the amorphous form $I_a r$ can account for the anomalous gas retention reported for warming of impure ices to temperatures $T > 150$ K (7, 30), because probably not all trapped volatiles are released until sublimation or transformation into hexagonal ice (I_h).

We conclude that the structural forms of amorphous water ice and their transitions underlie and are responsible for many hitherto "anomalous" properties of astrophysical ices. These findings allow remote observations of astrophysical ices to be interpreted in terms of structural properties of the water ice matrix.

REFERENCES AND NOTES

1. A. G. G. M. Tielens, in *Interstellar Dust*, L. J. Allamandola and A. G. G. M. Tielens, Eds. (International Astronomical Union, Santa Clara, CA, 1988), vol. 135, pp. 239–262; J. M. Greenberg, in *Chemistry in Space*, J. M. Greenberg and V. Pirronello, Eds. (Kluwer Academic, Dordrecht, Netherlands, 1991), pp. 227–261; M. C. Festou, H. Rickman, R. M. West, *Astron. Astrophys. Rev.* 5, 37 (1993).
2. M. J. Mumma, P. R. Weissman, S. A. Stern, in *Protostars and Planets III*, E. H. Levy, J. I. Lunine, M. S. Matthews, Eds. (Univ. of Arizona Press, Tucson, 1993), pp. 1177–1252.
3. H. G. Heide, *Ultramicroscopy* 14, 271 (1984); _____ and E. Zeitler, *ibid.* 16, 151 (1985).
4. M. G. Sceats and S. A. Rice, in *Water: A Comprehensive Treatise*, F. Franks, Ed. (Plenum, New York, 1982), vol. 7, pp. 83–214.
5. F. Sciortino, A. Geiger, H. E. Stanley, *J. Chem. Phys.* 96, 3857 (1992); *Nature* 354, 218 (1992).
6. A. Pohorille, L. R. Pratt, R. A. LaViolette, M. A. Wilson, R. D. MacElroy, *J. Chem. Phys.* 87, 6070 (1987); L. Jichen and D. K. Ross, *Nature* 365, 327 (1993).
7. A. Bar-Nun, G. Herman, D. Laufer, *Icarus* 63, 317 (1985); A. Kouchi and T. Kuroda, in *Proceedings of the 24th ESLAB Symposium on the Formation of Stars and Planets* (European Space Agency, Paris, 1990), vol. SP-315, pp. 193–196.
8. W. Hagen, A. G. G. M. Tielens, J. M. Greenberg, *Chem. Phys.* 56, 367 (1981).
9. S. A. Sandford and L. J. Allamandola, *Icarus* 76, 201 (1988); B. Rowland, M. Fisher, J. P. Devlin, *J. Chem. Phys.* 95, 1378 (1991).
10. D. F. Blake and G. Palmer, in *Microbeam Analysis–1991*, D. G. Howitt, Ed. (26th Microbeam Analysis Society Meeting) (San Francisco Press, San Francisco, CA, 1991), pp. 293–298.
11. We prepare the ice film by bleeding degassed

Fig. 4. A laboratory simulation of the formation of reduced organic matter ("organic residue") from a UV-photolyzed ice mixture $H_2O:CO:NH_3$ (0.63:0.25:0.12) deposited at 15 K (data by W. A. Schutte) (27). The figure shows the intensity of a number of infrared absorption bands that were monitored during warm-up at about 1 K per minute, where the band assignment to functional groups is that of Schutte (27). The structural transitions as derived from Figs. 2 and 3 are clearly seen in the changes in the infrared absorption spectra during warm-up.
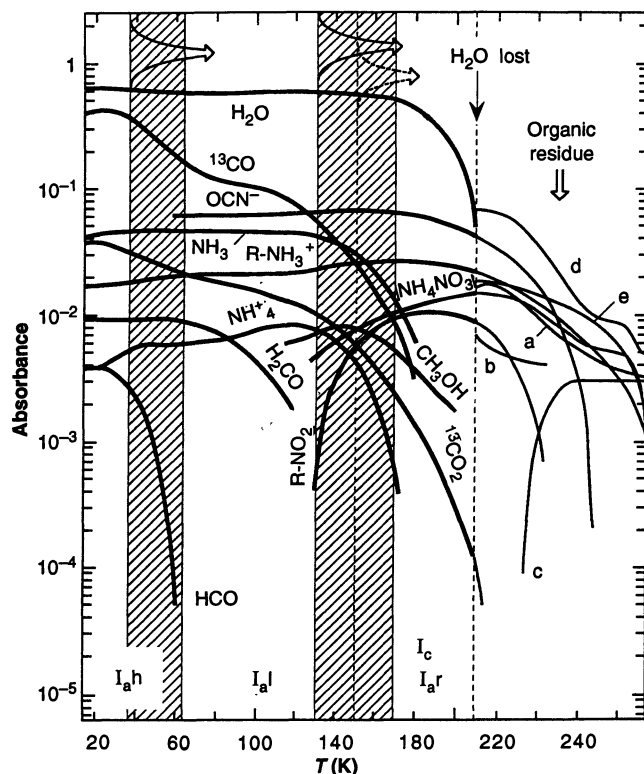
distilled water vapor from a gas reservoir at 14 torr and room temperature into the microscope until the partial H_2O pressure rises to 4×10^{-6} torr. We grow films of ice by opening for 10 s a shutter that covers the sample at all times when the ice is not viewed (rate of growth, 18 μm/hour). The resulting film is smooth and homogeneous. Bright-field imaging reveals no sign of crystallinity even at high magnification. There is no indication of needle or stalactite-like surface features, and the diffraction pattern directly after deposition does not show crystalline diffraction peaks for deposition temperatures below about 120 K. The form transitions are observed to occur simultaneously across the entire substrate. Low–electron dose imaging techniques minimize sample degradation during viewing. Electron beam damage does not change the diffraction patterns on time scales of each measurement, and we move to a different part of the ice layer in subsequent measurements.

12. A. H. Narten, C. G. Venkatesh, S. A. Rice, *J. Chem. Phys.* **64**, 1106 (1976).
13. T. C. Sivakumar, S. A. Rice, M. C. Sceats, *ibid.* **69**, 3468 (1978).
14. L. G. Dowell and A. P. Rinfret, *Nature* **188**, 1144 (1960).
15. A. Hallbrucker and E. Mayer, *Icarus* **90**, 176 (1991).
16. B. Schmitt, S. Espinasse, R. J. A. Grim, J. M. Greenberg, J. Klinger, in *Proceedings of the International Workshop on Physics and Mechanics of Cometary Materials*, T. D. G. J. Hunts, Ed. (European Space Agency, Paris, 1989), vol. ESA SP-302, pp. 65–69.
17. N. J. Sack and R. A. Baragiola, *Phys. Rev. B* **48**, 9973 (1993).
18. L. Pauling, *The Nature of the Chemical Bond* (Cornell Univ. Press, Ithaca, NY, 1960), chap. 12, pp. 449–504.
19. Our choice of nomenclature for the amorphous forms is given by the success of describing amorphous forms by random network models and follows previous suggestions to name the amorphous form I_v [J. Dubochet, J. Chang, R. Freeman, J. Lepault, A. W. McDowall, *Ultramicroscopy* **10**, 55 (1982)], I_{as} (21), or I_a (17). We prefer this notation to that used in studies related to liquid water, that is, $H_2O(as)$, $H_2O(as,l)$, or $(H_2O)_{as}$. Although the Roman numeral polymorph designations are generally applied only to the crystalline phases, the structure of the low-density amorphous form is well represented by a disordered ice I network and the high-density form by such a network including interstitial water. We believe that alternative models for high-density ice based on one of the 11 high-pressure phases of water (4, 12) are unlikely because they are either outside their stability regime or demand a form of proton ordering [B. Kamb, in *Water and Aqueous Solutions*, R. A. Horne, Ed. (Wiley-Interscience, New York, 1973), pp. 9–24]. Of course, we realize that an amorphous form may not have a unique structure. For example, the high-density form might have a varying content of interstitial water if deposition conditions vary. The justification for giving names to these forms is that there are well-defined transition zones between the different forms. Alternative amorphous forms have been made in the laboratory (and similarly bear some relation to ice I) by pressure-induced amorphosing hexagonal ice I_h at 77 K and 10 kbar [O. Mishima, L. D. Calvert, E. Whalley, *Nature* **310**, 393 (1984)]. This synthetic ice shows a similar high- to low-density transition, but at a higher temperature of 105 to 128 K [Y. P. Handa, O. Mishima, E. Whalley, *J. Chem. Phys.* **84**, 2766 (1986); A. Bizid, L. Bosio, A. Defrain, M. Oumezzine, *ibid.* **87**, 2225 (1987); J. Tse, *ibid.* **96**, 5482 (1992)].
20. L. C. Allen, in *Physics and Chemistry of Ice*, E. Whalley, S. J. Jones, L. W. Gold, Eds. (Royal Society of Canada, Ottawa, 1974), pp. 13–18.
21. A. Kouchi, *Nature* **330**, 550 (1987); *J. Cryst. Growth* **99**, 1220 (1990).
22. R. J. Speedy, *J. Phys. Chem.* **96**, 2322 (1992).

23. J. A. Ghormley, *J. Chem. Phys.* **48**, 503 (1968); A. Hallbrucker, E. Mayer, G. P. Johari, *J. Phys. Chem.* **93**, 7751 (1989).
24. A. G. G. M. Tielens, W. Hagen, J. M. Greenberg, *J. Phys. Chem.* **87**, 4220 (1983); G. A. Baratta and G. Stazzulla, *Astron. Astrophys.* **240**, 429 (1990).
25. J. M. Greenberg, A. J. Yencha, J. W. Corbett, H. L. Frisch, *Mem. Soc. R. Sci. Liege* **6e serie, tome III**, 425 (1972); W. Hagen, L. J. Allamandola, J. M. Greenberg, *Astrophys. Space Sci.* **65**, 215 (1979).
26. P. Jenniskens et al., *Astron. Astrophys.* **273**, 583 (1993).
27. W. A. Schutte, thesis, University of Leiden, Leiden, Netherlands (1988).
28. A. Kouchi and T. Kuroda, *Nature* **344**, 134 (1990).
29. M. Duncan, T. Quinn, S. Tremaine, *Astron. J.* **94**, 1330 (1987).
30. J. A. Ghormley, *J. Chem. Phys.* **46**, 1321 (1967).
31. We acknowledge the work of G. Palmer, who is responsible for a number of important modifications to the electron microscope, and A. Breon, who automated the reduction process of large batches of diffraction patterns. M. A. Wilson assisted in the analysis of the diffraction patterns. We thank W. A. Schutte for permission to reproduce figure III.1.4 from his thesis in Fig. 4. This report benefited from discussions with A. Pohorille, A. G. G. M. Tielens, L. J. Allamandola, F. Freund, and S. Chang. This work was supported by grants from the Exobiology and Planetary Materials and Geochemistry Programs of the National Aeronautics and Space Administration and was performed while P.J. held a National Research Council–Ames Research Center Research Associateship.

3 February 1994; accepted 20 June 1994

Infrared Laser Spectroscopy of the Linear C_{13} Carbon Cluster

T. F. Giesen,* A. Van Orden, H. J. Hwang,† R. S. Fellers, R. A. Provençal, R. J. Saykally

The infrared absorption spectrum of a linear, 13-atom carbon cluster (C_{13}) has been observed by the use of a supersonic cluster beam–diode laser spectrometer. Seventy-six rovibrational transitions were measured near 1809 wave numbers and assigned to an antisymmetric stretching fundamental in the $^1\Sigma_g^+$ ground state of C_{13}. This definitive structural characterization of a carbon cluster in the intermediate size range between C_{10} and C_{20} is in apparent conflict with theoretical calculations, which predict that clusters of this size should exist as planar monocyclic rings.

The structure and bonding in pure carbon molecules have been of interest for many years because of the importance of these species in many contexts, ranging from dust-grain formation in the interstellar medium to soot formation in combustion systems. Recently, this interest in carbon clusters has intensified because of the dramatic emergence of fullerene science, centered primarily about the discovery and characterization of the C_{60} molecule and other members of this "third form of carbon." A review article by Weltner and Van Zee describes research conducted before 1989 (1). Experimental (2) and theoretical (3) evidence suggests that the formation of C_{60} and other fullerenes proceeds by a mechanism in which small carbon clusters undergo condensation from linear chains through monocyclic rings and finally to large three-dimensional, cage-like structures. A detailed characterization of this mechanism, as well as those for related processes like soot formation, requires a thorough understanding of how the structure and bonding evolve in smaller carbon clusters as the cluster size increases.

Extensive theoretical and experimental efforts have been under way for several years to elucidate these mechanisms. From theoretical considerations, the picture that has emerged is that the small, odd-numbered clusters of C_3 to C_9 exist exclusively as cumulenic linear chains with $^1\Sigma_g^+$ ground electronic states, whereas the even-numbered clusters of C_4, C_6, and C_8 have two nearly isoenergetic structural isomers, a $^3\Sigma_g^-$ linear chain and a nearly planar singlet cyclic ring (4–6). Above C_9 a transition occurs, and the ground-state structures of both even and odd clusters become planar monocyclic rings, while the corresponding linear structures become relatively high in energy (5, 7, 8). This trend is thought to continue for C_{10} to C_{20}. As the cluster size increases toward C_{20}, high-level ab initio calculations become unfeasible, although several calculations at lower levels of theory have been reported (9, 10). Ion mobility measurements indicate that a rich variety of structures begins to form above C_{20}, including planar monocyclic and polycyclic rings (11). Some calculations suggest that clusters as small as C_{18} may exist as fullerenes (10), although there is no experimental evidence to support this suggestion. However, it is clear that fullerenes become the most stable structures at sizes larger than C_{30}.

Experimental verification of this picture

Department of Chemistry, University of California, Berkeley, CA 94720, USA.

*Present address: I. Physikalisches Institut, der Universität zu Köln, 50937 Köln, Germany.
†Present address: Department of Chemistry, Kyung Hee University, Seoul, 130-701, Korea.